CILAMCE 2017
Florianópolis - Santa Catarina - Brazil

# NUMERICAL METHODS OF PHASE SHIFTING TO STRESS MEASUREMENT WITH DIGITAL PHOTOELASTICITY USING PLANE POLARISCOPE


**Filipe Gomes Vieira**

**Jordana Simões Ribeiro Martins**

**Marcos Vinícius dos Santos Rocha**

**Tiago Augusto da Silva**

**Pedro Américo Almeida Magalhães Júnior**

filipe.gomes@sga.pucminas.br

martinsjsr@gmail.com

marcos-rocha-18@hotmail.com

tiago.vnbh@gmail.com

pamerico@pucminas.br

Pontifícia Universidade Católica de Minas Gerais, Department of Mechanical Engineering, Avenida Dom José Gaspar, 500 – Coração Eucarístico, Belo Horizonte – MG, 30535-901, Brazil.

**João Marcos Simões Ribeiro**

joaomarcos_87@hotmail.com

Centro Federal de Educação Tecnológica de Minas Gerais, Department of Mechanical Engineering, Rua José Peres, 558 – Centro, Leopoldina – MG, 36700-000, Brazil.



***Abstract.*** *The aim of this research work is to get numerical equations for the phase-shifting method in digital photoelasticity using a plane polariscope. The model was developed to plane polariscope because of the simplicity and low cost of this equipment. To develop the phase shift and respective intensity equations only the analyzer is rotated. A ring under diametral compression is used for the experimental validation. From these intensity equations, the equations for isoclinic and isochromatic parameters are deduced by applying a new numerical technique. This approach can be used to calculate the isoclinic and isochromatic parameters using any number of images. Several analysis are performed with different number of photographic images. The results showed errors reduce when more phase-stepped images are utilized. Hence, we conclude that the uncertainties in results due to* *effects of errors on photoelastic images can be reduced with a larger amount of phase-stepped images. The results are compared to a three-step method to improve its reliability.*

***Keywords:*** *Numerical Methods, Photoelasticity*

# INTRODUCTION

The photoelastic technique can be used for whole-field stress analysis in the materials that presents the property of temporary birefringence. The photoelasticity allows determination of the difference between the two principal stresses and the direction of the principal stresses, which are represented by the isochromatic and the isoclinic fringes. The phase-shifting method is one of the most widely used for whole-field analysis. In phase-shifting method, the intensity data for three or more different optical arrangements are recorded. Hence, the fractional fringe order at any point can be determined by the intensity data recorded at that point for various optical arrangements.

In phase-shifting algorithms, the change in phase is achieved by rotation of the optical elements of the polariscope. This requires that all optical elements in polariscope be able to rotate independently. Unfortunately, this is not the case for many commercially available polariscopes widely used in laboratories of industries and universities. The significant advantage of the methodology proposed in this paper is that the method only changes the angle of the analyzer in the polariscope and that one can obtain equations for estimating the phase for any number of images in various situations. The physical reason for the proposed numerical model is that the measurement uncertainty can be reduced by increasing the number of phase-stepped images.

Magalhães Jr, et al. (2009) and Magalhães Jr, et al. (2011) developed a generalization of a phase-shifting method used in moiré technique (Carre algorithm). This generalization made possible use any number of equations in phase evaluation and it led to reduction of the errors in phase calculus. Based on the generalization of Carre algorithm, a multistep phase-shifting algorithm for photoelasticity is developed to use in plane polariscopes.

Measurement uncertainty is a parameter characterizing the dispersion of the values attributed to a measured quantity. No measurement is exact, the uncertainty has probabilistic basis and reflects incomplete knowledge of the quantity. All the measurements are subject to uncertainty, and a measured value is only complete if a statement of the associated uncertainty accompanies it (Magalhães and Magalhães Jr., 2012). The new method can be used with any number of photoelastic measures in plane polariscope.

The main advantages of the plane polariscopes are immune to mismatch of quarter-wave plate, need fewer adjusts during experiments and reduce the chance of error because they have fewer optical elements than circular polariscopes. Furthermore, it was shown that plane polariscope based algorithms give better isoclinics values than the methods that use a quarter wave plate (Ramji and Ramesh, 2008) and (Ramji, et al., 2006). With better results in isoclinic values, it is possible to obtain less error in separation of stresses by the shear stress technique. For this reason, it is important to improve the technique elaborated in Magalhães and Magalhães Jr. (2012) initially developed for circular polariscope arrangement to extend it for the plane polariscope arrangement. Another possibility would be to use the two techniques for developing an analogous technique to ten-step method, which is the most adequate for use in manual polariscope based phase-shifting technique (Ramji and Prasath, 2011).

In this paper, a new method to overcome the limitation of positioning of the commercial polariscopes and to reduce errors in photoelastic measurements involving a new numerical model is suggested. A comparative study was made between the theoretical results and the numerical methodologies using a ring under diametral compression.

# 1 THE PHASE-SHIFTING METHODS

The plane polariscope is one of the simplest optical arrangements possible in photoelastic technique. The Fig. 1 shows the typical arrangement (Ramesh, 2000), where P, R and A represent polarizer, retarder (stressed model) and analyzer, respectively. The subscripts written after P and A means the angle between the polarizing axis and the reference axis x, for instance: $P_\alpha R_{\theta,\delta} A_\beta$ indicates that the polarizer is at α and analyzer is at an arbitrary angle β with x-axis. The subscripts δ and θ of R indicate the retardation added by stressed sample and whose fast axis is at angle θ with x-axis.

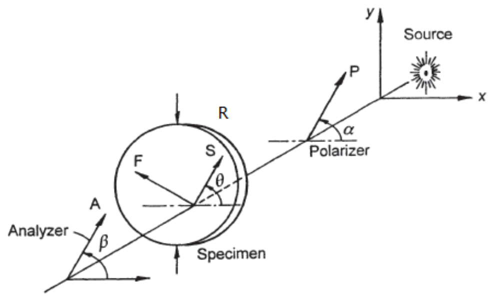


**Figure 1. Optical arrangement of a plane polariscope**

The optical elements of the polariscopes introduce rotation and retardation on the light waves. Using the Jones calculus any arrangement of the plane polariscope is obtained using the matrices operation. The output electric field for the arrangement $P_\alpha R_{\theta,\delta} A_\beta$, as shown in Fig. 1, both along and perpendicular to the analyzer axis ($E_\beta$, $E_{\beta+90°}$) are given as (Ramesh, 2000)

$$\begin{pmatrix} E_\beta \\ E_{\beta+90°} \end{pmatrix} = \begin{bmatrix} \cos\beta & \sin\beta \\ -\sin\beta & \cos\beta \end{bmatrix} \begin{bmatrix} \cos\frac{\delta}{2} - i\sin\frac{\delta}{2}\cos 2\theta & -i\sin\frac{\delta}{2}\sin 2\theta \\ -i\sin\frac{\delta}{2}\sin 2\theta & \cos\frac{\delta}{2} + i\sin\frac{\delta}{2}\cos 2\theta \end{bmatrix} \begin{pmatrix} \cos\alpha \\ \sin\alpha \end{pmatrix} K e^{i\omega t}, \quad (1)$$

where $i = \sqrt{-1}$. The symbols $K$ and $\omega$ are the amplitude and the angular frequency of the light vector, respectively. To find the output light intensity the following operation is made (Ramesh, 2000):

$$I = E_\beta E_\beta^* . \quad (2)$$

In Eq. (2), $I$ is the output light intensity and $E_\beta^*$ is the complex conjugate of $E_\beta$. After operation using Eq. (2), the output intensity emerging from analyzer of the polariscope arrangement $P_\alpha R_{\theta,\delta} A_\beta$ is given by (Ramesh, 2000)

$$I = I_o \left[ \left( \cos\frac{\delta}{2} \right)^2 (\cos(\beta-\alpha))^2 + \left( \sin\frac{\delta}{2} \right)^2 (\cos(\beta+\alpha-2\theta))^2 \right], \quad (3)$$

where $I_o$ accounts for the amplitude of incident light vector and the proportionality constant. The effect of background intensity is not explicitly taken into account by introducing a parameter $I_b$ in the intensity equation. Instead, we capture an image of an unstressed model when polarizer and analyzer are kept in crossed position. The intensity values of this image are to be subtracted from all other images before any processing is done (Ramesh, 2000).

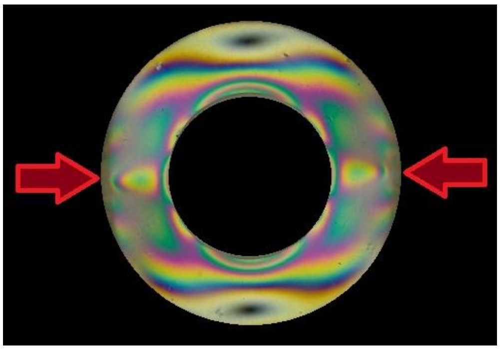

**Figure 2. Sample under compression**

In the experimental procedure, as shown in Fig. 2, the inner and the outer diameter and the thickness of the annular disk are $d$ = 38 mm, $D$ = 75 mm and $t$ = 6 mm, respectively. A diametrically opposite load, $p$ = 50 N is applied on the annular disk. An epoxy resin with stress fringe value $F$ = 296 N/mm is used. In photoelastic analysis, the theoretical value of isochromatic $\delta$ is related to two principal stress components, $\sigma_1$ and $\sigma_2$, as in Eq. (4) (Magalhães and Magalhães Jr., 2012). The theoretical isoclinic angle $\theta$ can be calculated using Eq. (5) with stress components $\sigma_x$, $\sigma_y$ and $\tau_{xy}$ (Magalhães and Magalhães Jr., 2012) in the range $-\pi$ to $+\pi$.

$$\delta = \frac{2\pi \cdot t}{F}(\sigma_1 - \sigma_2), \tag{4}$$

$$\theta = \frac{1}{2}\tan^{-1}\left(\frac{2\tau_{xy}}{\sigma_x - \sigma_y}\right). \tag{5}$$

By elasticity theory, the exact expression of the stress field in polar coordinates, as a function of $r$ and $\varphi$ with its origin at the center of disk, is as follows (Tokovyy, et al., 2010):

$$\sigma_r^e = \frac{p}{\pi}\left[-\frac{\rho^2 - k^2}{1-k^2}\frac{2\Theta}{\rho^2} + \sum_{m=1}^{\infty}\frac{(-1)^m R_m(\rho)}{m}\sin(2m\Theta)\cos(2m\varphi)\right], \tag{6}$$

$$\sigma_\varphi^e = \frac{p}{\pi}\left[-\frac{\rho^2 - k^2}{1-k^2}\frac{2\Theta}{\rho^2} + \sum_{m=1}^{\infty}\frac{(-1)^m \Phi_m(\rho)}{m}\sin(2m\Theta)\cos(2m\varphi)\right], \tag{7}$$

$$\tau_{r\varphi}^e = \frac{p}{\pi}\sum_{m=1}^{\infty}\frac{(-1)^m S_m(\rho)}{m}\sin(2m\Theta)\cos(2m\varphi), \tag{8}$$

where $e$ means exact result, $p$ is the pressure applied to ring, $\Theta$ is the angle of application of pressure, $\rho = r/R_1$ and $k = R_1/R_2$ with $r$, $R_1$, $R_2$ equal to an arbitrary radius, the internal radius and the external radius of the ring, respectively. The functions of ρ are

$$R_m(\rho)=\left(2(m+1)\rho^{-2m}-(2m+1)k^2\rho^{-2(1+m)}-k^{2(1-2m)}\rho^{-2(1-m)}\right)A_m \\ -\left(2(m-1)\rho^{2m}-(2m-1)k^2\rho^{-2(1-m)}+k^{2(1+2m)}\rho^{-2(1+m)}\right)B_m \quad , \tag{9}$$

$$\Phi_m(\rho)=\left((2m+1)k^2\rho^{-2(1+m)}-2(m-1)\rho^{-2m}+k^{2(1-2m)}\rho^{-2(1-m)}\right)A_m \\ -\left((2m-1)k^2\rho^{-2(1-m)}-2(m+1)\rho^{2m}-k^{2(1+2m)}\rho^{-2(1+m)}\right)B_m \quad , \tag{10}$$

$$S_m(\rho)=\left(2m\rho^{-2m}-(2m+1)k^2\rho^{-2(1+m)}+k^{2(1-2m)}\rho^{-2(1-m)}\right)A_m \\ +\left(2m\rho^{2m}-(2m-1)k^2\rho^{-2(1-m)}-k^{2(1+2m)}\rho^{-2(1+m)}\right)B_m \quad , \tag{11}$$

the constants of integration $A_m$ and $B_m$ have the form

$$A_m=\frac{k^{2(1+m)}\left(k^{2m}-k^{-2m}\right)-2m\left(1-k^2\right)}{4m^2\left(1-k^2\right)^2-k^2\left(k^{2m}-k^{-2m}\right)^2}, \tag{12}$$

$$B_m=\frac{2m\left(1-k^2\right)-k^{2(1+m)}\left(k^{2m}-k^{-2m}\right)}{4m^2\left(1-k^2\right)^2-k^2\left(k^{2m}-k^{-2m}\right)^2}. \tag{13}$$

With these equations $\sigma_1$, $\sigma_2$ and $\theta$ can be obtained as follows

$$\sigma_{1,2}^e=\frac{\sigma_r+\sigma_\varphi}{2}\pm\sqrt{\left(\frac{\sigma_r-\sigma_\varphi}{2}\right)^2+\sigma_{r\varphi}^2}\ , \tag{14}$$

$$\theta^e=\frac{1}{2}\tan^{-1}\left(\frac{(\sigma_r-\sigma_\varphi)\sin(2\varphi)+2\sigma_{r\varphi}\cos(2\varphi)}{(\sigma_r-\sigma_\varphi)\cos(2\varphi)-2\sigma_{r\varphi}\sin(2\varphi)}\right). \tag{15}$$

The change of polar coordinates to Cartesian coordinates is given by

$$\sigma_{xx}^e=\sigma_{rr}\cos^2(\varphi)+\sigma_{\theta\theta}\sin^2(\varphi)-\tau_{r\theta}\sin(2\varphi), \tag{16}$$

$$\sigma_{yy}^e=\sigma_{rr}\sin^2(\varphi)+\sigma_{\theta\theta}\cos^2(\varphi)+\tau_{r\theta}\sin(2\varphi), \tag{17}$$

$$\tau_{xy}^e=(\sigma_{rr}-\sigma_{\theta\theta})\cos(\varphi)\sin(\varphi)+\tau_{r\theta}\cos(2\varphi). \tag{18}$$

Thus, using Eqs. (4) and (5), the exact value of $\delta$ and $\theta$ can be calculated at each point in an annular disk. We have compared the experimental measurements of $\delta$ and $\theta$, obtained from the proposed method in this research, with its exact values to test the new equations as shown in Magalhães and Magalhães Jr. (2012).

## 2 THE PROPOSED MODEL

Using the same principle of the mathematical model proposed in Magalhães and Magalhães Jr. (2012), we propose a new methodology for generating the equations of phase obtained by comparing it with the conventional form to obtain equations of phase involving the plane polariscope. The general numerical equations for estimating the photoelastic parameters with any number $N$ of images is proposed as follows:

$$\theta = \frac{1}{2}\tan^{-1}\left(\frac{\sum_{j=1}^{N} b_j I_j}{\sum_{j=1}^{N} c_j I_j}\right), \tag{19}$$

$$\delta = \cos^{-1}\left(\frac{\cos 2(\theta-\alpha)\left(\sin 2\theta \sum_{j=1}^{N} d_j I_j + \cos 2\theta \sum_{j=1}^{N} e_j I_j\right)}{\sin 2(\theta-\alpha)\left(\cos 2\theta \sum_{j=1}^{N} f_j I_j + \sin 2\theta \sum_{j=1}^{N} g_j I_j\right)}\right), \tag{20}$$

where $N$ is the number of images, $b_j$, $d_j$ and $e_j$ are the coefficients of numerator, $c_j$, $f_j$ and $g_j$ are coefficients of denominator, and $j$ is the index of the sum. Based on the mathematical model developed in Magalhães and Magalhães Jr. (2012), Eq. (19) for isoclinic angle $\theta$ and Eq. (20) for isochromatic parameter $\delta$ has been deduced.

To use the Eqs. (19) and (20), the coefficients $b_j$, $d_j$, $e_j$, $c_j$, $f_j$ and $g_j$ must be determined. How the chosen values for these coefficients are very important to final results, we developed two optimization models to calculate the coefficients that would give a small amount of error in the numerical solution (error $\leq 10^{-6}$). Thus, we do not try to obtain the most optimized coefficients because get coefficients that give a small error in numerical solution would be sufficient to achieve the objective of this research. The optimization models are shown in Eqs. (21) and (22). A set of coefficients shall be calculated for each set of angles and numbers of images. These optimization models are easy to solve because they involve linear programming and a maximized solution can be obtained using the simplex method. The processing time for the solution of this mathematical model is very fast, even using personal computers, the solution is given in few seconds.

The shift from obtaining equations for calculating the phase analytically to obtaining them numerically is a significant innovation. It breaks a paradigm that was hitherto used by several authors (Ramji and Prasath, 2011) and (Ramesh, 2000). After several attempts, the following optimization models were identified for calculating the coefficients for the numerical equations:

$$
\begin{aligned}
&\textit{Maximize} \quad \sum_{j=1}^{N} b_j + c_j \\
&\textit{subject to} \quad \begin{cases}
& \qquad\qquad\qquad\qquad\qquad \text{Quantities} \\
1) & \tan(2\theta^v)\sum_{j=1}^{N} c_j.I_j^v = \sum_{j=1}^{N} b_j.I_j^v \qquad v > 2N \\
2) & -1 \le b_j \le 1, \quad -1 \le c_j \le 1 \qquad j = 1..N \\
3) & b_j, \ \ \mathrm{c_j} \text{ are real numbers} \qquad j = 1..N
\end{cases}
\end{aligned}
$$

where for each *v*:

$$
\begin{cases}
I_j^v = I_o^v.\left[\cos^2\left(\dfrac{\delta^v}{2}\right).\cos^2\left(\beta_j - \alpha\right) + \sin^2\left(\dfrac{\delta^v}{2}\right).\cos^2\left(\beta_j + \alpha - 2.\theta^v\right)\right], \ j = 1..N \\
I_o^v \in [0;\ \ 255] \quad \text{random and real} \\
\theta^v \in [-\pi/4;\ \ \pi/4] \quad \text{random and real} \\
\delta^v \in [0;\ \ \pi] \quad \text{random and real} \\
\beta_j = \dfrac{2\pi}{3}\left(\dfrac{j-1}{Step-1}\right) - \dfrac{\pi}{3} \qquad , \ j = 1..N
\end{cases}
$$

$step = [3,4,5,6,7,9,11,13,16,21,25,31,41]$ or integer values greater than 3

$N =$ number of images from 3 until the step value , (21)

$j = 1..N$

$\beta_j =$ analyzer angle

$\alpha =$ polarizer angle = 60°

$\theta =$ isoclinic angle

$\delta$ = isochromatic parameter

$$
\begin{array}{ll}
Maximize & \sum_{j=1}^{N} d_j + e_j + f_j + g_j \\
subject\ \ \text{to} & \begin{cases}
 & & \text{Quantities} \\
1) & \cos(\delta^v)\sin\left[2.\left(\theta^v-\alpha\right)\right].\left[\cos(2.\theta^v).\sum_{j=1}^{N} f_j.I_j^v+\sin(2.\theta^v).\sum_{j=1}^{N} g_j.I_j^v\right]= & v>2N \\
 & \cos\left[2.\left(\theta^v-\alpha\right)\right].\left[\sin(2.\theta^v).\sum_{j=1}^{N} d_j.I_j^v+\cos(2.\theta^v).\sum_{j=1}^{N} e_j.I_j^v\right] & \\
2) & -1\le b_j\le 1, \quad -1\le c_j\le 1 & j=1..N \\
3) & d_j,\ \ \mathrm{e_j},\ \ \mathrm{f_j},\ \ \mathrm{g_j}\ \ \text{are real numbers} & j=1..N
\end{cases}
\end{array}
$$

where for each $v$:

$$
\begin{cases}
I_j^v = I_o^v.\left[\cos^2\left(\dfrac{\delta^v}{2}\right).\cos^2\left(\beta_j-\alpha\right)+\sin^2\left(\dfrac{\delta^v}{2}\right).\cos^2\left(\beta_j+\alpha-2.\theta^v\right)\right], j=1..N \\
I_o^v \in [0;\ 255] \quad r\text{andom and real} \\
\theta^v \in [-\pi/4;\ \pi/4] \quad r\text{andom and real} \\
\delta^v \in [0;\ \pi] \quad r\text{andom and real} \\
\beta_j = \dfrac{2\pi}{3}\left(\dfrac{j-1}{Step-1}\right)-\dfrac{\pi}{3} \qquad , j=1..N
\end{cases}
$$

$$
\begin{array}{l}
step = [\,3,4,5,6,7,9,11,13,16,21,25,31,41\,]\ \ or\ \text{int}eger\ \ values\ \ greater\ \ than\ 3 \\
N = number\ of\ \ images\ \ from\ 3\ until\ the\ step\ de\ value \\
j = 1..N \\
\beta_j =\ analyzer\ \ angle \\
\alpha = polarizer\ \ \ angle = 60° \\
\theta = isoclinic\ \ \ angle \\
\delta = isochromatic\ \ \ parameter
\end{array}
\qquad (22)
$$

The optimization models above maximize the coefficients of numerator ($b_j$, $d_j$, $e_j$) and the coefficients of denominator ($c_j$, $f_j$, $g_j$) in both Eqs. (19) and (20). Therefore the obtained values for them are large enough to be significant in Eqs. (19) and (20). The *step* represents values greater than or equal to 3. $N$ is the number of images and is an integer number between 3 and the value of *step*. The *step* value was created to define the angular step of the analyzer and always give integer angles values to the angular steps, $step \geq N$ to avoid repeated angles.

The constraints 1 in Eqs. (21) and (22) are made so that all coefficients generate correct values for the estimation of $\theta$ and $\delta$. To ensure that one has a hyperrestricted problem, we suggest that the number of greater restrictions must be at least equal to the number of variables (Magalhães and Magalhães Jr., 2012).

The constraints 2 and 3 in Eqs. (21) and (22) indicate that the coefficients are real numbers smaller than one and greater than negative one, thus error propagation are avoided. For the need to evaluate phase, these limiting factors will increase the values of intensity $I_o$ that contains errors due to noise and improve discretization in pixels and in shades of gray (Magalhães and Magalhães Jr., 2012).

In the optimization model the values of $I_o$ is limited between 0 and 255, $\theta$ is limited between $-\pi/4$ and $\pi/4$, $\delta$ is limited between 0 and $\pi$. The *step* value defines the distance between the angles measured in analyzer. The angular step is given by (60° - (-60°)) / (*step*-1). Table 1 shows the coefficients obtained when $N$ = 5, *step* = 5, $\alpha$ = 60° and the angles of the analyzer ($\beta$) as follows: -60°, -30°, 0°, 30°, 60°.

Table 1. Values of the real coefficients ($b_j$, $c_j$, $d_j$, $e_j$, $f_j$, $g_j$) when $N$ = 5 and *step* = 5

| j | $\beta_j$ | $b_j$ | $c_j$ | $d_j$ | $e_j$ | $f_j$ | $g_j$ |
|---|---|---|---|---|---|---|---|
| 1 | -60° | -0.92265 | 1.00000 | 0.52073 | 1.00000 | 0.18916 | 1.00000 |
| 2 | -30° | 1.00000 | 1.00000 | 1.00000 | 0.00000 | -0.55519 | 1.00000 |
| 3 | 0° | 1.00000 | 0.66667 | 1.00000 | -1.00000 | -1.00000 | 1.00000 |
| 4 | 30° | 0.38675 | -1.00000 | 0.09808 | -1.00000 | -0.54289 | -1.00000 |
| 5 | 60° | -0.30940 | 0.33333 | -0.88675 | 0.00000 | 0.17686 | 1.00000 |

The Table 2 shows the coefficients for $N$ = 4, *step* = 4, $\alpha$ = 60° and the angles of the analyzer ($\beta$) as follows: -60°, -20°, 20°, 60°.

Table 2. Values of the real coefficients ($b_j$, $c_j$, $d_j$, $e_j$, $f_j$, $g_j$) when $N$ = 4 and *step* = 4

| j | $\beta_j$ | $b_j$ | $c_j$ | $d_j$ | $e_j$ | $f_j$ | $g_j$ |
|---|---|---|---|---|---|---|---|
| 1 | -60° | -0.35775 | 1.00000 | 1.00000 | 1.00000 | 0.03389 | 1.00000 |
| 2 | -20° | 0.78017 | 1.00000 | 1.00000 | -0.88429 | -0.58004 | 1.00000 |
| 3 | 20° | 1.00000 | -0.38333 | 0.44337 | -1.00000 | -1.00000 | -0.17877 |
| 4 | 60° | -0.52091 | -0.05520 | -0.79058 | -0.06995 | 0.34560 | 0.25820 |

Table 3 shows the coefficients for $N$ = 3, *step* = 5, $\alpha$ = 60° and the angle $\beta$ as follows: -60°, -30°, 0°. Unlike the other, in Table 3, step is two units greater than $N$, therefore, the angles with the same absolute value and opposite sign to the first two angles are not present.

Table 3. Values of the real coefficients ($b_j$, $c_j$, $d_j$, $e_j$, $f_j$, $g_j$) when $N$ = 3 and *step* = 5

| j | $\beta_j$ | $b_j$ | $c_j$ | $d_j$ | $e_j$ | $f_j$ | $g_j$ |
|---|---|---|---|---|---|---|---|
| 1 | -60° | -0.57735 | 0.33333 | -0.23020 | 0.08932 | 0.57735 | 0.82137 |
| 2 | -30° | 0.57735 | 1.00000 | 1.00000 | 0.39872 | -0.57735 | 1.00000 |
| 3 | 0° | 0.57735 | -0.33333 | -0.19245 | -0.82137 | -1.00000 | -0.08932 |

Table 4 shows the coefficients obtained when $N$ = 3, *step* = 6, $\alpha$ = 60° and $\beta$ as follows: -60°, -36°, -12°. The coefficients in Tables (1-4) are examples that can be used in Eqs. (19) and (20) to implement the phase shifting technique.

Table 4. Values of the real coefficients ($b_j$, $c_j$, $d_j$, $e_j$, $f_j$, $g_j$) when $N$ = 3 and *step* = 6

| j | $\beta_j$ | $b_j$ | $c_j$ | $d_j$ | $e_j$ | $f_j$ | $g_j$ |
|---|---|---|---|---|---|---|---|
| 1 | -60° | -0.31280 | 0.07072 | -0.02148 | 0.19321 | 0.29647 | 0.18332 |
| 2 | -36° | -0.06876 | 1.00000 | 1.00000 | 0.28965 | 0.15770 | 1.00000 |
| 3 | -12° | 0.82678 | -0.29956 | -0.26397 | -0.89540 | -1.00000 | -0.23792 |

To verify the new equations for calculating phase (Eqs. (19) and (20)), a computer program was created that generates random values of $I_o$, $\theta$' and $\delta$', as same procedure mentioned in Magalhães and Magalhães Jr. (2012). With Eq. (3) are calculated $N$ values of $I_j$ to each value of $\beta_j$, then the new phase equations were applied on the values of $I_j$ to determine whether they produced correct values of $\theta$ and $\delta$. The calculations of the accuracy was performed one hundred thousand of times for each equation in phase calculation. At least 99.999% of time, we obtain the accuracy ($|\theta' - \theta|$ $|\delta' - \delta|$) $\leq 10^{-6}$. The models of Eqs. (19) and (20) were tested until *step* and $N$ equals 2000, the value at which the increment $\Delta\beta$ would be 0.05°. The unwrap process was performed after we obtain $\theta$ and $\delta$ between [-π, π]. This process consists in add or subtract $2\pi$ at each discontinuity encountered in the phase data. The unwrapping procedure consists of finding the correct field for each phase measurement (Magalhães and Magalhães Jr., 2012).

## 3 RESULTS AND DISCUSSION

For analysis the annular disk under diametric compression, we used a pixel number of 1024 × 1024 in the digitization, a grey level between 0 and 255 and a white light source. Figure 3 shows a flowchart of processing to phase-shifting method applied.

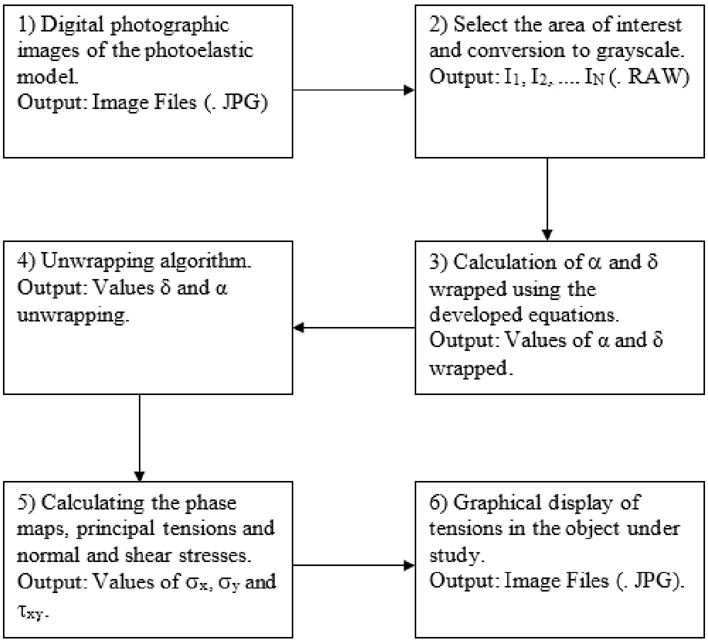


**Figure 3. Flowchart showing each processing stage**

The new equations was tested in the experimental procedures using a ring under diametral compression whose exact solution is known, thus we could evaluate the average relative error comparing the experimental and exact results using Eqs. (23) and (24).

$$E_\theta = \frac{1}{M}\sum_{i=1}^{M}\frac{\left|\theta_i^e - \theta_i\right|}{\left|\theta_i^e\right|}, \tag{23}$$

$$E_\delta = \frac{1}{M}\sum_{i=1}^{M}\frac{\left|\delta_i^e - \delta_i\right|}{\left|\delta_i^e\right|}, \tag{24}$$

where, the Eqs. (23) and (24) represent the average relative error $E_\theta$ and $E_\delta$ for the parameters $\theta$ and $\delta$, respectively. $M$ is the number of pixels of the image and $\theta_i^e$ and $\delta_i^e$ are the exact values calculated by Eqs. (4)-(18) for the ring, $\theta_i$ and $\delta_i$ are calculated with Eqs. (19) and (20). This comparison process was made for a number of images between 3 and 41, for analysis of error in the numerical method.

To compare the new equations for calculating the phase many sets of images with step values equal to 3, 4, 5, 6, 7, 9, 11, 13, 16, 21, 25, 31, and 41 were generated. The data in these tables confirms that the average error decreases when the number of images increases. In Magalhães and Magalhães Jr. (2012), they noted that for a same number of images, the average error increases when the variation of the angle $\beta$ between the images decreases, but not able to explain the possible origins of this trend.

We believe that this trend can be induced due to *step* $\geq N$ means not all the pairs of angles of opposite signs are employed as in the conventional method, for instance, $N = 3$ and *step* = 5 gives $\beta_i$ = -60°, -30°, 0°; that is, lacking the angles 30° and 60°. Therefore, the error increases as there is no equivalence between the intensity equations.

In Magalhães and Magalhães Jr. (2012) it was noted that for each equation developed, the average errors in the angle $\delta$ are larger than the errors found in the angle $\theta$ of the isoclinic fringes and it was associated with an absolute value $\delta$ greater than $\theta$. It can be verified with Figs. 4 and 5, as the percentage error in $\theta$ and $\delta$ are almost the same in most of the data, this affirmation may be correct.

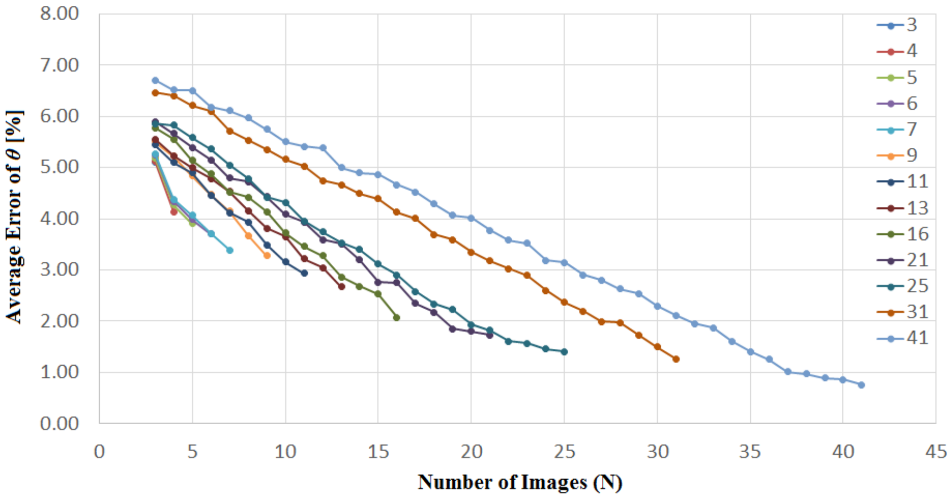


**Figure 4. Average error of θ**

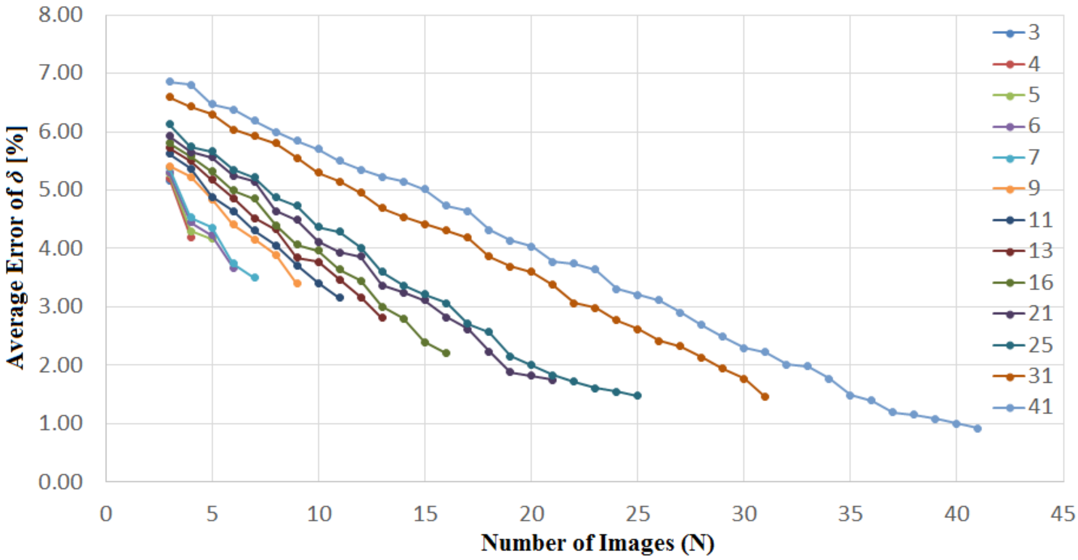


**Figure 5. Average error of $\delta$**

The errors in the results could be explained for misalignments in the optical elements during the experimental procedures, dust in the lenses of the polariscope, small defects on the photoelastic models, changes in environment illumination, errors in edges due to wide stress variation, non-uniform load distributions over the model. These error sources combined with the limit of resolution of photographic camera worsen the image quality and interfere on the results of image processing.

After the obtained values of $\theta$ and $\delta$ unwrapping (Plouzennec and Lagarde, 1999) and (Pinit and Umezaki, 2008) the shear stress difference technique for whole field stress separation is employed. Thus, it calculates the principal stresses, normal stresses, phase maps, shear stresses and the von Mises stress. Thereafter, graphical displays of stresses in the ring are displayed.

A comparison between a three-step conventional algorithm (Sarma, et al., 1992) and the numerical approach was made. The conventional algorithm gave $E_\theta$ = 3.11% and $E_\delta$ = 2.78%. To achieve these values was implemented the same process applied on the numerical approach, only the phase shifting technique was different. This result shows that the numerical approach can overcome the accuracy of the conventional algorithm when more than thirteen images are used. Despite using more images in analysis, the numerical approach can be useful when a high precision is required or when the polariscope has limiting angular position. From Figs. 4 and 5, the new method gives $E_\theta$ = 2,67% and $E_\delta$ = 2.82% when using 13 images. Thus, to reach the results of this conventional algorithm four times more images were necessary. Therefore, the new method developed in this research is most appropriate in measurements that demands greater accuracy or when measurements are made in polariscopes with limitations in the angular position of the optical elements, which prevents the use of conventional algorithms.

# 4 CONCLUSION

In this research, two numerical equations to implement the phase-shifting technique in plane polariscope was developed. We conclude that increasing the number of images the average error decrease, this is an advantage over the conventional method. In the results, it is observed that the method gives better results when $N = step$, because, in this case, we use only pairs of angles with same absolute value and opposite sign. When $N \neq step$, errors are added during the processing of the equations in estimating $\theta$ and $\delta$, as this increases the average error.

The main advantage of the approach numerical over the conventional method is it can used in any polariscope commercially available, eliminating the needs for dedicated equipment to the experimental procedures. Furthermore, the new method facilitates the automatization of the analysis because only the analyzer is rotated for acquiring the photographic images. The results of the research indicate that the method gives fewer errors and so is applicable to experimental stress or analysis.

With the new approach, it was possible to develop a photoelastic system that moves the analyzer of the plane polariscope at a constant speed while a camera takes many pictures at equal intervals of time. With this technique, the measurements are more precise and there are fewer uncertainties. The photoelastic technique has seen some renewed interest in past few years with digital images and image processing new methods becoming readily available. However, further research is needed to improve the precision, the accuracy and the automation of photoelastic technique.

## ACKNOWLEDGEMENTS

The authors thank the financial support of the Conselho Nacional de Desenvolvimento Científico e Tecnológico (CNPq), the Fundação de Amparo à Pesquisa de Minas Gerais (FAPEMIG), the Coordenação de Aperfeiçoamento de Pessoal de Nível Superior (CAPES) and the Pontifícia Universidade Católica de Minas Gerais (PUC Minas).

## REFERENCES

Dally J. W., Rilley W. F., 2005. *Experimental stress analysis*. College House Enterprises, Knoxville, pp.55-80.

Magalhães C. A., 2011. Ph. D. thesis, Pontificia Universidade Católica de Minas Gerais, Belo Horizonte.

Magalhães C. A., Magalhães Jr P. A. A., 2012. New numerical methods for the photoelastic technique with high accuracy. *Journal of Applied Physics* 112, 083111.

Magalhães Jr P. A. A., Smith Neto P. and Barcellos C. S. de, 2011. Generalization of Carré equation. Optik 122, pp. 475-489.

Magalhães Jr P. A. A., Smith Neto P. and Barcellos C. S. de, 2009. Phase shifting technique using generalization of Carre algorithm with many images. Optical Review 16(4), pp. 432-441.

Ramji M., Prasath R. G. R., 2011. Sensivity of isoclinic data using various phase shifting techniques in digital photoelasticity towards generalized error sources. *Optics and Lasers in Engineering* 49, pp. 1153-1167.

Ramesh K., 2000. *Digital photoelasticity: advanced techniques and applications*. Springer-Verlag, Berlin.

Tokovyy Yu. V., Hung K. M., Ma C. C., 2010. Determination of stresses and displacements in a thin annular disk subject to diametral compression. *Journal of Mathematical Sciences* 165, pp. 342-354.

Plouzennec N., Lagarde A., 1999. Two-wavelength method for full-field automated photoelasticity. *Experimental Mechanics* 39(4), pp. 274-277.

Pinit P., Umezaki E., 2008. Absolute fringe order determination in digital photoelasticity. *Journal of Solid Mechanics and Materials Engineering* 2(4), pp. 519-529.

Sarma A. V. S. S. S. R., Pillai S. A., Subramanian G., Varadan T. K., 1992. Computadorized image processing for whole-field determination of isoclinics and isochromatics. *Experimental Mechanics* 32(1), pp. 24-29.